Journal of Materials Chemistry A

Accepted Manuscript

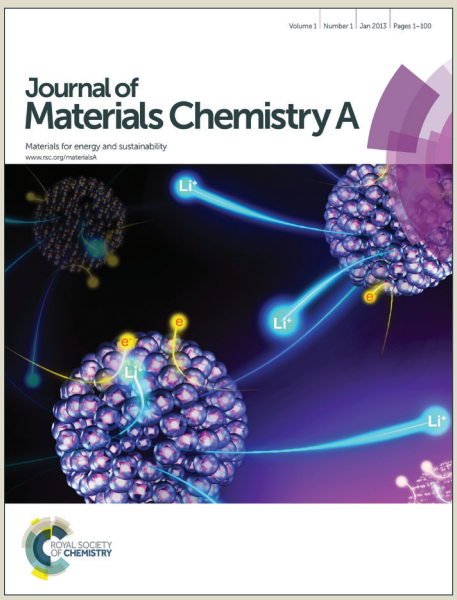

ROYAL SOCIETY OF CHEMISTRY

www.rsc.org/materialsA

Ordered mesoporous C/TiO_2 composites as advanced sonocatalysts

Pengpeng Qiu[1], Wei Li[2], Kyounglim Kang[1], Beomguk Park[1], Wei Luo[2], Dongyuan Zhao[2]*, and Jeehyeong Khim[1]*

[1]School of Civil Environmental and Architecture Engineering, Korea University, Seoul 136-701, Republic of Korea

[2]Laboratory of Advanced Materials and Department of Chemistry, Fudan University, Shanghai 200433, China

E-mail: hyeong@korea.ac.kr, dyzhao@fudan.edu.cn

Ordered mesoporous C/TiO_2 composites have been fabricated *via* an evaporation induced co-assembly method, and demonstrated as a highly efficient sonocatalyst. The effects of carbon content in the composites and calcination temperature have been investigated thoroughly in this work and optimized for the production of well-defined mesoporous C/TiO_2 materials. The resultant composites possess superior "brick-mortar" frameworks with uniform TiO_2 nanocrystals glued by carbon matrix, and exhibit highly ordered mesostructures with high surface areas (~ 200 m^2/g). More importantly, the mesoporous C/TiO_2 composites show a high sonocatalytic degradation rate of Rhodamine B. The maximum pseudo first-order reaction rate constant obtained with the composites 15C-85TiO_2-450 (C: 15.2 wt%, TiO_2: 84.8 wt%, calcined at 450 °C) is 0.178 min^{-1}, which is 2.7 and 4.8 times higher than that of P25 (0.062 min^{-1}) and ultrasound (0.037 min^{-1}) alone, respectively. The excellent sonocatalytic performance is a result of fast mass diffusion, enhanced nucleation rate and rapid surface hydroxyl radical oxidation. In addition, the recycling test shows that the sonocatalytic degradation rate with 15C-85TiO_2-450 is retained even after five cycles, which is related to the well-retained mesostructure with superior

mechanical stability. We believe that the present results provide important insights for the design and synthesis of advanced sonocatalysts.

Introduction

Advanced oxidation processes (AOPs) have emerged as an efficient technology for the destruction and mineralization of organic pollutants through powerful reactive oxidation species such as hydroxyl radicals. As an alternative to conventional AOPs such as ozonation,[1] photolysis,[2] Fenton process[3] and photocatalytic oxidation,[4, 5] sonolysis is of great interest owing to its environment-friendly and simple operation. In sonolysis, acoustic cavitation including the nucleation, growth, and collapse of microbubbles occurs, leading to the generation of sonoluminescence and "hot spots" with extremely high temperatures (5000 K) and pressures (1000 atm).[6] As a result, water is dissociated to generate hydroxyl radicals, which can oxidize organic pollutants into CO_2 and H_2O. However, to obtain a fast ultrasonic degradation rate by using onefold ultrasound (US) typically requires a significant amount of electric energy, costly equipment, and long irradiation time. To overcome the drawbacks, heterogeneous sonocatalyst is critical and promising. Among various sonocatalysts, TiO_2-based materials are widely investigated because of their good photocatalytic properties, nontoxicity, and cost-effectiveness.[7, 8] More importantly, it has been demonstrated that TiO_2-based materials exhibited high sonocatalytic activities due to the synergistic effects between US and TiO_2.[9-13] For example, Song *et al*.,[12] prepared La-doped TiO_2, which showed a high sonocatalytic degradation rate of amaranth. Zou *et al*.,[13] have reported the synthesis of CeO_2-modified TiO_2 as a sonocatalyst and the reaction rate was 3.3 times as high as that of ultrasound alone. Zhang, Kubo and coworkers described that the sonocatalytic degradation rate of organic pollutants in the presence of activated carbon/TiO_2 composites was 1.2 and 1.5 times higher than that of P25, respectively.[14,

[15] However, the small pore size and disordered microporous structure of activated carbon greatly hinder the mass transfer and adsorption process.[16] What' more, TiO_2 nanocrystals were supported in the pores of activated carbon, causing pore trapping, which further reduced the sonocatalytic activity.

Recently, ordered mesoporous materials have been received increasing attention because of their fascinating properties such as regular, uniform and interpenetrating mesopores, large pore sizes, high surface areas as well as abundant framework compositions.[17-20] Compared with their bulk counterparts, they can interact with atoms, ions, molecules or even larger guest species not only at the external surface, but also in the whole internal pore system. As a result, ordered mesoporous materials exhibit substantial performance boosts in numerous applications such as adsorption, separation, catalysis, drug delivery, and so on.[21] However, up to date, the investigation of ordered mesoporous materials as sonocatalysts has not been reported yet.

Herein, ordered mesoporous C/TiO_2 composites have been fabricated *via* an evaporation-induced co-assembly (EISA) method, and demonstrated as a highly efficient catalyst for enhancing ultrasonic degradation rate of organic pollutants. The synthetic parameters such as the content of carbon and crystalline temperature have been investigated thoroughly in this work and optimized for the production of ordered mesoporous C/TiO_2 composites. The resultant composites possess superior "brick-mortar" frameworks with uniform TiO_2 nanocrystals glued by carbon, and exhibit well-ordered mesostructures with high surface areas (~ 200 m^2/g). The resultant mesoporous C/TiO_2 composites are used as sonocatalysts for degradation of Rodomine B (RhB), and exhibit a high degradation rate (0.178 min^{-1}), which is 2.7 and 1.5 times as high as that of mesoporous TiO_2 (0.062 min^{-1}) and carbon (0.122 min^{-1}) alone, respectively. More importantly, this performance is much better than those for C/TiO_2 sonocatalysts reported

previously, which is possibly caused by the enhanced synergistic effects between carbon and TiO_2. Moreover, the ordered mesoporous C/TiO_2 catalysts can be easily recycled and exhibit approximately constant activity even after 5 cycles.

Experimental Section

Materials

Triblock poly(ethylene oxide)-*b*-poly (propylene oxide)-*b*-poly(ethylene oxide) copolymer Pluronic P123 ($EO_{20}PO_{70}EO_{20}$, Mw = 5800) and Rhodamine B (RhB) were purchased from Sigma-Aldrich (USA). Titaniumtetrachloride ($TiCl_4$, > 98.0 %), tetrabutyl orthotitanate (TBOT, > 98.0 %), phenol (C_6H_5OH, 99.98 %), formalin (HCHO, 37.0 – 40.0 wt%), hydrogen chloride (HCl, 36.5 wt%), sodium hydroxide (NaOH, > 96.0 %), and ethanol (C_2H_5OH, > 99.7 %) were obtained from the Shanghai Chemical Company (China). Millipore water was used in all experiments.

Preparation of ordered mesoporous C/TiO_2 composites

The C/TiO_2 composites were synthesized by the method reported previously,[22, 23] using $TiCl_4$ and $Ti(OC_4H_9)_4$ as the mixed titanium sources,[24] phenolic resins as a carbon source, and Pluronic P123 as the structure-directing agent. In a typical synthesis, 0.70 g of $TiCl_4$, 2.1 g of $Ti(OC_4H_9)_4$, and 1.2 g of preformed phenolic resins in an ethanolic solution that contained 0.144 g of phenol and 0.264 g of formaldehyde were added into a clear solution of 1.0 g of P123 and 20 g of ethanol, respectively. After 10 min, the mixture was poured into dishes. Then, the dishes were placed under a hood to evaporate ethanol at ambient temperature for 6 h and in an oven to thermopolymerize at 100 °C for 12 h. The orange samples were collected and heated at 350 °C for 2 h to remove the template. Crystallization of titania was carried out at 450, 550, 650, and 750 °C for 2 h under nitrogen. The heating rate was 1 °C/min below 350 °C and 5 °C/min above

350 °C. The overall synthetic scheme is shown in Fig. S1. The carbon content in the composites could be tuned by adjusting the amount of phenolic resin. The obtained samples were denoted as *x*C-(100 – *x*)TiO_2-y, where *x* represents the mass percentage of theoretical added carbon and y represents the calcination temperature.

For comparison, mesoporous TiO_2 was prepared by calcining the as-made 30C-70TiO_2 sample at 450 °C for 2 h under air to burn out carbon. The resultant sample was denoted as M-TiO_2-450. Mesoporous carbon was prepared by a similar procedure.[25] First, Pluronic P123 (1.0 g) was dissolved in 20 g of ethanol under vigorous stirring. Then, 6.0 g of phenolic resol was added and the solution was stirred for another 10 min. Finally, the mixture was transferred into the dishes and placed in a hood to evaporate ethanol for 6 h. Thermopolymerization was carried out in an oven for 48 h at 100 °C. The as-made orange sample was collected and heated at 450 °C for 2 h. The resultant sample was denoted as C-450.

Characterizations

Small-angle X-ray scattering (SAXS) measurements were recorded on a Nanostar U small-angle X-ray scattering system (Bruker, Germany) using Cu Kα radiation (40 kV, 35 mA). X-ray diffraction (XRD) patterns were recorded on a Bruker D8X-ray diffractometer with Ni-filtered Cu Kα radiation (40 kV, 40 mA). Nitrogen sorption isotherms were measured at 77 K with a Micromeritics Tristar 3020 analyzer (USA). Prior to measurements, the samples were degassed in a vacuum at 180 °C for 6 h. The Brunauer-Emmett-Teller (BET) method was utilized to calculate the specific surface areas (S_{BET}) using adsorption data in the relative pressure range P/P_0 = 0.04 – 0.2. Using the Barrett-Joyner-Halenda (BJH) model, the pore size distributions were derived from the adsorption branches of the isotherms, and the total pore volumes (V) were estimated from the adsorbed amount at the relative pressure P/P_0 of 0.995. Transmission electron

microscopy (TEM) was carried out on a JEOL 2011 microscope (Japan) operated at 200 kV. For TEM measurements, the sample was suspended in ethanol and supported on a holey carbon film on a Cu grid. Thermogravimetric analysis (TGA) was carried out on a Mettler Toledo TGASDTA851 analyzer (Switzerland) from 30 to 700 °C under air with a heating rate of 5 °C/min.

Sonocatalytic degradation measurement

The sonoreactor consisted of a glass-cup–horn-type container with a capacity of 1.25 L (Φ 10.0× 16.0 cm), and was equipped with a cup–horn-type ultrasonic transducer (Mirae Ultrasonic MEGA-100) (Fig. S2). The frequency was 300 kHz and the maximum power (100 W) was applied using a single piezoelectric transducer (Tamura). A 200-mL beaker (Φ 6.0 × 10.0 cm) was emerged into the container loaded with 250 mL of water for the reaction. The height of liquid level in the container was ~ 3 cm. The solution temperature was measured using a thermometer (Tecpel DTM-318) and maintained with a water jacket. A retort stand was used to fix the emerged beaker. The distance between the bottom of the beaker and container was about 1 cm. Aqueous suspensions (30 mL) of RhB (50 mg/L) and C/TiO_2 composites (1.0 g/L) were used for the sonocatalytic degradation. At given time intervals, 0.60 mL of the suspension was removed using a 5-mL syringe and filtered by a membrane with a pore size of ~ 0.45 μm. Furthermore, 3.0 mL of a diluted solution was prepared by dissolving 0.50 mL of the filtered sample into 2.5 mL of water. The diluted solution was analyzed by recording the variations of the absorption band maximum (554 nm) using a ThermoSpectronic UV 500 UV-visible spectrometer.

Adsorption test and hydroxyl radical measurement

Adsorption kinetic experiments were carried out to assess the adsorption rate with varied sonocatalysts. For a typical experiment, aqueous suspensions (30 mL) of RhB (50 mg/L) and sonocatalyst (1.0 g/L) were mixed in a 200-mL beaker and agitated under 500 rpm in a thermo stated rotary shake at 12 °C. In addition, the sample collection and analysis are same as that used in sonocatalytic degradation experiments. The detection of generated H_2O_2 was used as an indirect method to measure the concentration of hydroxyl radicals, which was described by Beckett and Hua *et al*.,[26] Typically, 1000 mL of A solution dissolved with KI (66 g), NaOH (2.0 g) and $(NH_4)_6Mo_7O_{24}{\cdot}4H_2O$ (2.0 g), and 1000 mL of B solution containing 10 g of $C_6H_4COOKCOOH$ was prepared and stirred for 24 h. A mixed solution of 0.25 mL/0.5 mL/0.25 mL (A solution/sample/B solution) was added to a 10-mL tube orderly. The mixed solution was diluted by adding 3.0 ml of water and stirred quickly for 10 sec before the absorbance was measured. The concentration of H_2O_2 was measured at absorption band maximum of 350 nm using the ThermoSpectronic UV 500 UV-visible spectrometer.

Results and discussion

Characterization of the C/TiO_2 composites

The SAXS pattern (Fig. 1A) of the as-made sample 30C-70TiO_2 showed three resolved scattering peaks, which could be indexed to the 10, 11, and 20 reflections of 2D hexagonal symmetry (space group of *p6mm*), suggesting a highly ordered mesostructure. After calcination for 2 h at 450 °C under N_2, three resolved diffraction peaks were still observed, suggesting that the hexagonal ordered structure was retained (Fig. 1A). However, the peaks became less resolved due to the removal of the templates and the formation of anatase nanocrystals in the frameworks during the calcination. The mesostructures were gradually degraded as the carbon content decreased (Fig. 1A). It illustrates that the carbon matrix can prevent the structural reconstruction,

thus avoiding framework collapses during calcination. The resultant carbon contents in the 5C-95TiO_2-450, 10C-90TiO_2-450, 15C-85TiO_2-450, 20C-80TiO_2-450, and 30C-70TiO_2-450 composites through TGA analyses were 7.74, 10.59, 15.16, 22.14, and 29.28 wt%, respectively (Fig. S3), which were similar with the adding amounts. SAXS patterns of 15C-85TiO_2 samples (Fig. 1B) became gradually less resolved and the intensities of diffraction peaks greatly decreased with increasing the calcination temperature from 450 to 750 °C. When being calcined at 750 °C for 2 h, all the peaks of the samples disappeared in the SAXS pattern, indicating a complete collapse of the mesostructure, which might be caused by the continuous growth of TiO_2 nanocrystals in the pore walls at a high temperature (Table 1).

The XRD pattern (Fig. 2A) of mesoporous TiO_2 (M-TiO_2-450) showed seven broad diffraction peaks at 2θ = 25.3, 37.4, 48.0 53.9/55.1, 62.7, 68.8/70.3, 75.0°, respectively, which can be well indexed as the 101, 004, 200, 105/211, 204, 116, and 215 reflections of anatase phase. Similar to the sample M-TiO_2-450, XRD patterns of the mesoporous C/TiO_2 composites with varied carbon content (Fig. 2A) displayed the characteristic peaks of anatase phase, suggesting the formation of anatase nanocrystals after calcination at 450 °C. In addition, with increasing carbon content, the intensities of the diffraction peaks decreased, indicating that the crystallinity of TiO_2 was weakened. It verifies that the amorphous carbon can inhibit the grain growth of TiO_2. The size of TiO_2 nanocrystals (Table 1) in the composites was calculated to be in the range of 5 – 7 nm and decreased with the rise of carbon content, which were smaller than that of M-TiO_2-450 (12.4 nm). XRD patterns of the sample 15C-85TiO_2 samples (Fig. 2B) showed that the diffraction peaks became intense and narrow by increasing the calcination temperature from 450 to 750 °C. In addition, rutile phase occurred when the calcination temperature is

beyond 650 °C. The inhibition of the phase transformation (from anatase to rutile) is due to the presence of amorphous carbon matrix.[27, 28]

The TEM image of the sample 15C-85TiO_2-450 revealed uniform well-ordered hexagonal channel arrays in large domains (Fig. 3A), which was consistent with the results from SAXS patterns. Energy-dispersive X-ray (EDX) of the 15C-85TiO_2-450 (Fig. S4) clearly showed the characteristic peaks of titanium, carbon, and oxygen, suggesting the coexistence of TiO_2 and carbon. In addition, the results of EDX indicated that the weight of C and the sum of Ti and O were 17.74 and 83.26 wt%, respectively, which was similar to the data obtained from TGA. High-resolution TEM (HRTEM) images (Fig. 3B) clearly showed that well-defined nanocrystals were embedded in the pore walls glued by amorphous carbon, further suggesting the formation of brick-mortar frameworks. A lattice fringe with a *d*-spacing of 0.35 nm was clearly observed (Fig. 3B) on the surface of nanocrystals, which corresponded to the (101) plane of anatase TiO_2.[29] In addition, the size of TiO_2 nanocrystals was approximately 5.4 nm. TEM images of the sample 30C-70TiO_2-450 also showed highly ordered hexagonal mesochannel arrays in large areas (Fig. 3C**)** and less thrusting of TiO_2 nanocrystals was observed (Fig. 3D). In contrast, the sample 10C-90TiO_2-450 composites possessed relatively less ordered mesoporous structures (Fig. S5A) and the thrusting of anatase TiO_2 nanocrystals became apparent (Fig. S5B). When being calcined at 650 °C, the resultant 15C-85TiO_2-650 composites showed worm-like mesoporous structure (Fig. S5C). HRTEM images of the 15C-85TiO_2-650 (Fig. S5D) clearly showed that large TiO_2 nanocrystals were thrusted into the mesochannels, thus blocking the pores. These results reveal that the carbon component can not only promote the self-assembly as-made into highly ordered mesophases, but also restrict the grain growth of TiO_2 and maintain the ordered mesoporous structures during the removal of surfactants at high temperatures.

N_2 sorption isotherms (Fig. 4A) of the mesoporous C/TiO_2 composites showed characteristic IV curves with H_2-type hysteresis loops,[29] related to imperfect cylinder channels presumably driven by growth of anatase nanocrystals within pore walls. The pore sizes of the mesoporous C/TiO_2 composites calculated from the adsorption data using the BJH model were in the range of 3.8 – 5.6 nm (Table 1 and Fig. 4B) and decreased as the rise of carbon content. That is because the TiO_2 "brick" can efficiently prevent the carbon framework shrinkage during the calcination process. The BET surface areas of the mesoporous C/TiO_2 composites were calculated to be in the range of 140 – 210 m^2/g. As the carbon content increased, the specific surface area and pore volume increased (Table 1). This phenomenon was reasonable because amorphous carbon possessed a relatively high surface area than that of dense TiO_2 nanoparticles. N_2 sorption isotherms (Fig. S6A) of the sample 15C-85TiO_2 calcined at different temperatures showed that H_2-type hysteresis loops were less resolved as the calcination temperature increasing from 450 to 750 °C whereas the corresponding pore size increased (Fig. S6B), which was probably resulted from the gradual collapse of the mesostructure into nanoparticle-aggregated form.

Sonocatalytic degradation of RhB

The effect of carbon content in the resultant composites on the sonocatalytic degradation of RhB was investigated (Fig. 5A and B). As a control, the sonocatalytic performance of US alone and P25 were also tested, exhibiting the degradation rate constants of 0.037 and 0.062 min^{-1}, respectively, when a pseudo first-order reaction was assumed. It further verifies that P25 can act as a good sonocatalyst for enhancing the ultrasonic degradation of RhB.[8] Pure mesoporous TiO_2 showed a comparable result to that of P25 with a degradation rate constant of 0.063 min^{-1}. When introducing carbon in the mesoporous composites, the sonocatalytic degradation rate of RhB (Fig. 5A and B) first increased with the rise of carbon content in C/TiO_2 composites. A maximum

sonocatalytic degradation rate was observed in the presence of the sample 15C-85TiO_2-450 (0.178 min^{-1}), which was 2.7 times higher that of the commercial TiO_2 nanoparticles (P25) and 4.8 times higher than that of US alone, respectively. Moreover, RhB was completely removed in 40 min (Fig. 5B). The performance is much better than those of the TiO_2-based sonocatalysts reported previously.[14, 15] We found that further increasing carbon content beyond 15.2 % did not lead to any further increase in the sonocatatlytic reaction rate, and even caused a decrease. The sonocatalytic degradation rate constants of RhB for the composites 20C-80TiO_2-450 and 30C-70TiO_2-450 were 0.172 and 0.159 min^{-1}, respectively. When pure mesoporous carbon (C-450) was used as the catalyst, a degradation rate constant of 0.122 min^{-1} was obtained, which is much smaller than that of the composite 15C-85TiO_2-450 (0.178 min^{-1}). However, the adsorption kinetic plot (Fig. 5C) revealed that the adsorption rate of RhB on mesoporous carbon (86 % loss in 1 h) was much higher than that of the composite 15-85TiO_2-450 (70 % loss in 1 h), which suggested the strong adsorption effect of carbon towards RhB molecules. It was also found that the adsorption rate increased as the rise of carbon content in the resultant composites and all were higher than that of P25. The measurements of generated hydroxyl radicals in the sonocatalytic system (Fig. 5D) confirm that TiO_2 nanocrystals in the presence of the mesoporous composites play a catalytic role for the degradation of RhB. More importantly, the maximum production rate of hydroxyl radicals was also obtained with the composite 15C-85TiO_2-450 (1.92×10^{-2} min^{-1}), which was much larger than that of P25 (7.0×10^{-3} min^{-1}). Interestingly, when increasing the carbon content, the hydroxyl-radical-production rate first increased at carbon content of less than 15.2 % and then decreased, suggesting that the TiO_2 nanocrystals would be fully encapsulated by amorphous carbon, thus reducing the active sites for the production of hydroxyl radicals during the sonocatalytic process. [30]

The sonocatalytic reaction rate constants of 15C-85TiO_2-450, 15C-85TiO_2-550, 15C-85TiO_2-650, and 15C-85TiO_2-750 composites (Fig. 6A, and B) were calculated to be 0.178, 0.164, 0.094, and 0.081 min^{-1}, respectively, indicating that an increased calcination temperature had a negative effect. The decrease in the sonocatalytic degradation of RhB is related to the decreased adsorption rate (Fig. 6C) and hydroxyl radical generation rate (Fig. 6D). Clearly, the adsorption rate of RhB on the mesoporous C/TiO_2 composites decreased with the rise of calcination temperature from 450 to 750 °C, which was possibly resulted from the collapsed pore structures and decreased BET surface areas, thus retarding the mass transfer and reducing the active sites for RhB adsorption. The hydroxyl-radical-production rates of the composites 15C-85TiO_2-450, 15C-85TiO_2-550, 15C-85TiO_2-650, and 15C-85TiO_2-750 were 1.92×10^{-2}, 1.76×10^{-2}, 1.65×10^{-2}, and 1.0×10^{-2} min^{-1}, respectively. The significant reduction may be attributed to the growth of TiO_2 grain and the phase transformation. Although high crystalline TiO_2 could facilitate the production of hydroxyl radicals,[31] the simultaneous collapsed ordered mesostructures would greatly reduce the nucleation rate of microbubbles, thus decreasing the cavitation effect.[32, 33] In this case, lower sonocatalytic performances at high calcination temperature indicate that an ordered mesostruture possess more important roles than the crytallinity of TiO_2 does.

The recycling test of the composite 15C-85TiO_2-450 was conducted (Fig. S7). After five recycles, a similar reaction rate constant was retained. The excellent reusability of the sample 15C-85TiO_2-450 was ultimately related to the well retained mesostructure after each cycle (Fig. S8A and B). TEM images clearly showed that the ordered mesoporous channels were well retained even after five cycles, suggesting the excellent mechanical stability of 15C-85TiO_2-450. The surface of the recycled sample became rough relative to fresh one, which was resulted from

the continuous pitting by the shock waves.[6] However, the pure mesoporous TiO_2 showed a poor mechanical stability (Fig. S9C-F). After ultrasonic treatment for five hours, the framework of the mesoporous TiO_2 was completely broken, indicating a strong adhesion effect of amorphous carbon toward TiO_2 nanocrystals in the composites. The reusability tests further confirm that the ordered mesoporous titaina-carbon composites are promising candidates as sonocatalysts.

The excellent performances of the ordered mesoporous C/TiO_2 composites for sonocatalytic degradation of RhB may be attributed to the synergistic effect of their textual properties, as illustrated in Fig. 7. First, the presence of carbon component not only provides a "glue" effect to stabilize anatase TiO_2 nanocrystals, thus producing well-ordered mesostructures with a high mechanical stability (Fig. 3 and Fig. S8), but also greatly enhance the adsorption of RhB (Fig. 5C) due to their mutual affinities, which would be beneficial for surface hydroxyl radical oxidation induced by exposed TiO_2 nanocrystals in the pore walls. Additionally, the large pore size and ordered mesopores favored the mass transfer between aqueous and solid phases.[34, 35] Second, nucleation of a microbubble within a pore is faster than that of a flat or smooth surface because pore corners provide energetically preferred binding sites at which the new phase can be hold.[32, 33, 36] Therefore, the mesoporous C/TiO_2 composites provide large amount of nucleation sites for the generation of microbubbles, thus producing superior cavitation effects to irregular nanoparticles. Finally, the sonoluminescence and heat emitted by the collapsed bubbles could excite TiO_2 nanocrystals to form electron-holes pairs on the surface, which further promote the formation of reactive oxidation species in the reaction system.[37,38] Therefore, the high sonocatalytic performance of the composites 15C-85TiO_2-450 was a result of fast mass diffusion, enhanced nucleation rate and rapid surface hydroxyl radical oxidation.

Conclusions

Ordered mesoporous C/TiO_2 composites have been fabricated via an EISA method, and used as a highly efficient sonocatalyst. The effect of carbon content in the composites and calcination temperature have been investigated thoroughly in this work and optimized for the production of ordered mesoporous C/TiO_2 composites. The resultant composites possess superior "brick-mortar" frameworks with uniform TiO_2 nanocrystals glued by amorphous carbon, and exhibit well ordered mesostructures with high surface areas (~ 200 m^2/g). The resultant mesoporous C/TiO_2 composites possess high sonocatalytic degradation rates of RhB. The maximum pseudo first-order reaction rate constant obtained with the composites 15C-85TiO_2-450 is 0.178 min^{-1}, which is 2.7 and 4.8 times higher than that of P25 and ultrasound alone, respectively. The sonocatalytic degradation rate of RhB with the sample 15C-85TiO_2-450 can be retained even after five cycles. The excellent reusability is related to the well-retained mesostructure with superior mechanical stability. This study paves a promising way to design and synthesize advanced sonocatalysts.

Acknowledgments

This work was supported by the Basic Science Research Program through a National Research Foundation of Korea (NRF) grant funded by the Ministry of Education, Science, and Technology (KRF-2009-0092799). It also was supported by NSF of China (21210004), State Key Basic Research Program of the PRC (2012CB224805, 2013CB934104), Science and Technology Commission of Shanghai Municipality (08DZ2270500, 10JC1401800), and Shanghai Leading Academic Discipline Project (B108).

References

1. Y. Yamamoto, E. Niki and Y. Kamiya, *J. Org. Chem.*, 1981, **46**, 250-254.
2. C. Kormann, D. W. Bahnemann and M. R. Hoffmann, *Environ. Sci. Technol.*, 1991, **25**. 494-500.
3. Y. W. Kang and K. Y. Hwang, *Water Res.*, 2000, **34**, 2786-2790.

4. C. Minero, G. Mariella, V. Maurino and E. Pelizzetti, *Langmuir*, 2000, **16**, 2632-2641.
5. M. R. Prairie, L. R. Evans, B. M. Stange and S. L. Martinez, *Environ. Sci. Technol.*, 1993, **27**, 1776-1782.
6. K. S. Suslick, S. J. Doktycz and E. B. Flint, *Ultrason.*, 1990, **28**, 280-290.
7. M. F. Dadjour, C. Ogino, S. Matsumura and N. Shimizu, *Biochem. Eng. J.*, 2005, **25**, 243-248.
8. N. Shimizu, C. Ogino, M. F. Dadjour, K. Ninomiya, A. Fujihira and K. Sakiyama, *Ultrason. Sonochem.*, 2008, **15**, 988-994.
9. Y. Wang, D. Zhao, W. Ma, C. Chen and J. Zhao, *Environ. Sci. Technol.*, 2008, **42**, 6173-6178.
10. S. Zhang, *Ultrason. Sonochem.*, 2012, **19**, 767-771.
11. Y. Zhai, Y. Li, J. Wang, J. Wang, L. Yin, Y. Kong, G. Han and P. Fan, *J. Mol. Catal. A: Chem.*, 2013, **366**, 282-287.
12. L. Song, C. Chen, S. Zhang and Q. Wei, *Ultrason. Sonochem.*, 2011, **18**, 1057-1061.
13. M. Zou, Y. Kong, J. Wang, Q. Wang, Z. Wang, B. Wang and P. Fan, *Spectrochim. Acta, Part A*, 2013, **101**, 82-90.
14. Z. Zhang, Y. Xu, X. Ma, F. Li, D. Liu, Z. Chen, F. Zhang and D. D. Dionysiou, *J. Hazard. Mater.*, 2012, **209–210**, 271-277.
15. M. Kubo, H. Fukuda, X. J. Chua and T. Yonemoto, *Ind. Eng. Chem. Res.*, 2007, **46**, 699-704.
16. X. Zhuang, Y. Wan, C. Feng, Y. Shen and D. Zhao, *Chem. Mater.*, 2009, **21**, 706-716.
17. W. Li, Z. Wu, J. Wang, A. A. Elzatahry and D. Zhao, *Chem. Mater.*, 2013, **26**, 287-298.
18. W. Li, Q. Yue, Y. Deng and D. Zhao, *Adv. Mater.*, 2013, **25**, 5129-5152.
19. H. Oveisi, S. Rahighi, X. Jiang, Y. Nemoto, A. Beitollahi, S. Wakatsuki, and Y. Yamauchi, *Chem. Asian J.*, 2010, **5**, 1978-1983.
20. Y. Li, B. P. Bastakoti, M. Imura, S. M. Hwang, Z. Sun, J. H. Kim, S. X. Dou and Y. Yamauchi, *Chem. Eur. J.*, 2014, **20**, 6027-6032.
21. W. Li and D. Zhao, *Chem. Commun*., 2013, 49, 943-946.
22. X. Qian, Y. Wan, Y. Wen, N. Jia, H. Li and D. Zhao, *J. Colloid Interface Sci.*, 2008, **328**, 367-373.
23. R. Liu, Y. Ren, Y. Shi, F. Zhang, L. Zhang, B. Tu and D. Zhao, *Chem. Mater.*, 2007, **20**, 1140-1146.
24. B. Tian, X. Liu, B. Tu, C. Yu, J. Fan, L. Wang, S. Xie, G. D. Stucky and D. Zhao, *Nat. Mater.*, 2003, **2**, 159-163.
25. Y. Meng, D. Gu, F. Zhang, Y. Shi, H. Yang, Z. Li, C. Yu, B. Tu and D. Zhao, *Angew. Chem. Int. Ed.*, 2005, **117**, 7215-7221.
26. M. A. Beckett and I. Hua, *J. Phys. Chem. A.*, 2001, **105**, 3796-3802.
27. J. Zhang, Q. Xu, Z. Feng, M. Li, and C. Li, Angew. Chem. Int. Ed. 2008, **47**, 1766-1769
28. C. H. Huang, D. Gu, D. Zhao and R. A. Doong, Chem. Mater. 2010, **22**, 1760-1767.
29. W. Li, F. Wang, S. Feng, J. Wang, Z. Sun, B. Li, Y. Li, J. Yang, A. A. Elzatahry, Y. Xia and D. Zhao, *J. Am. Chem. Soc*., 2013, 135, 18300-18303.
30. Y. Yu, J. C. Yu, J. G. Yu, Y. C. Kwok, Y. K. Che, J. C. Zhao, L. Ding, W. K. Ge and P. K. Wong, *Appl. Catal. A: Gen.*, 2005, **289**, 186-196.
31. J. Wang, T. Ma, Z. H. Zhang, X. D. Zhang, Y. F. Jiang, D. B. Dong, P. Zhang and Y. Li, *J. Hazard. Mater*.,2006, **B137**, 972-980.
32. L. O. Hedges and S. Whitelam, *Soft Matter*, 2013, **9**, 9763-9766.

33. S. I. Madanshetty and R. E. Apfel, *J. Acoust. Soc. Am.*, 1991, **90**, 1508-1514.
34. W. Wei, C. Yu, Q. Zhao, X. Qian, G. Li and Y. Wan, *Appl. Catal., B: Environ.*, 2014, **146**, 151-161.
35. W. Wei, C. Yu, Q. Zhao, G. Li and Y. Wan, *Chem. Eur. J.*, 2013, **19**, 566-577.
36. A. J. Page and R. P. Sear, *Phys. Rev. Lett*., 2006, 97, 065701.
37. H. Ogi, M. Hirao and M. Shimoyama, *Ultrason.*, 2002, **40**, 649-650.
38. J. Mizuguchi and T. Shinbara, *J. Appl. Phys.*, 2004, **96**, 3514-3519.

Table 1. Physicochemical properties of the mesoporous C/TiO_2 composites prepared with different carbon contents and calcination temperatures.

Sample Name	a_0 (nm)	D_A (nm)	D (nm)	S_{BET} (m^2/g)	V (cm^3/g)
P25	8.24	13.6	-	50	0.065
M-TiO_2-450	8.19	12.4	6.32	84	0.122
5C-95TiO_2-450	8.17	6.2	5.65	145.69	0.132
10C-90TiO_2-450	8.16	5.9	5.43	158.30	0.139
15C-85TiO_2-450	8.17	5.8	5.31	169.94	0.145
20C-80TiO_2-450	8.20	5.6	4.85	186.91	0.156
30C-70TiO_2-450	8.15	5.2	3.99	224.61	0.257
15C-85TiO_2-550	8.16	6.7	3.54	235.87	0.150
15C-85TiO_2-650	8.17	8.5	3.59	247.82	0.175
15C-85TiO_2-750	8.86	9.2	3.69/7.81	186.76	0.285
C-450	-	-	3.54	657.20	0.42

a_0, unit-cell parameter; D_A, the particle size of anatase nanocrystals calculated by Scherrer formula; S_{BET}, BET surface area; **D**, pore-size diameter; **V**, total pore volume.

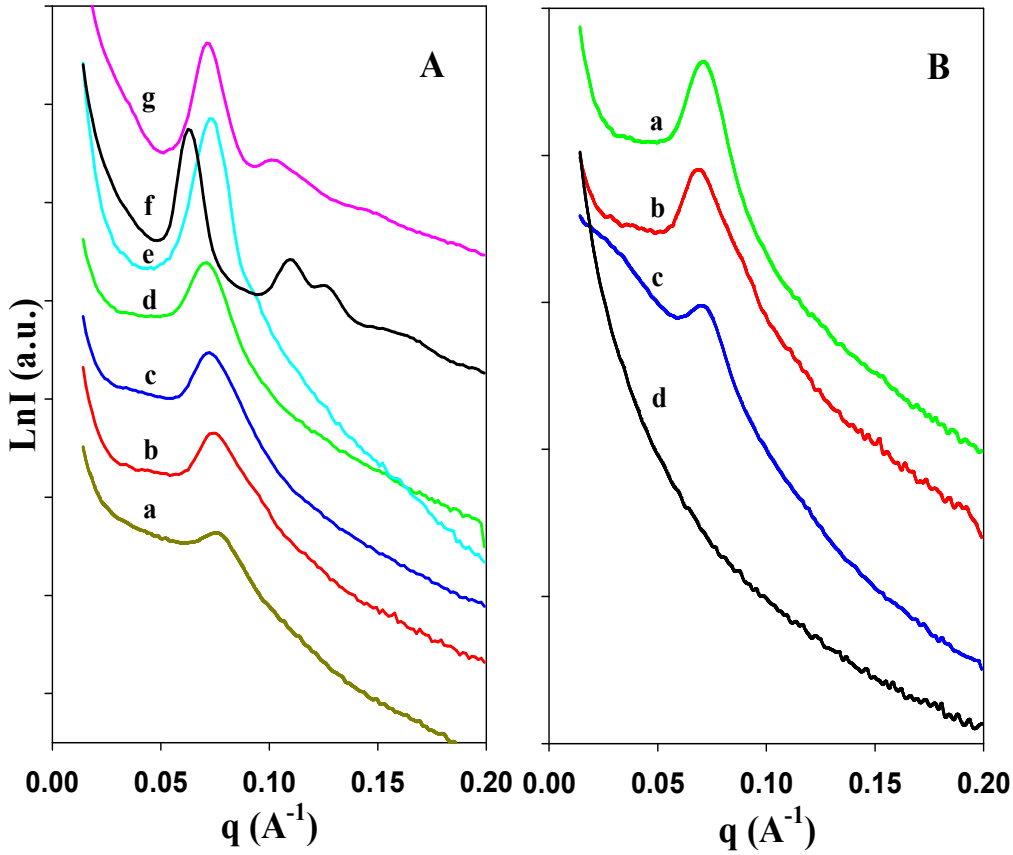

Fig. 1 (A) SAXS patterns of the mesoporous C/TiO_2 composites calcined at 450 °C with varied carbon content: (a) M-TiO_2-450, (b) 5C-95TiO_2-450, (c) 10C-90TiO_2-450, (d) 15C-85TiO_2-450, (e) 20C-80TiO_2-450, (f) 30C-70TiO_2-as made, (g) 30C-70TiO_2-450 and (B) SAXS patterns of the sample 15C-85TiO_2 calcined at different temperatures: (a) 15C-85TiO_2-450, (b) 15C-85TiO_2-550, (c) 15C-85TiO_2-650, (d) 15C-85TiO_2-750.

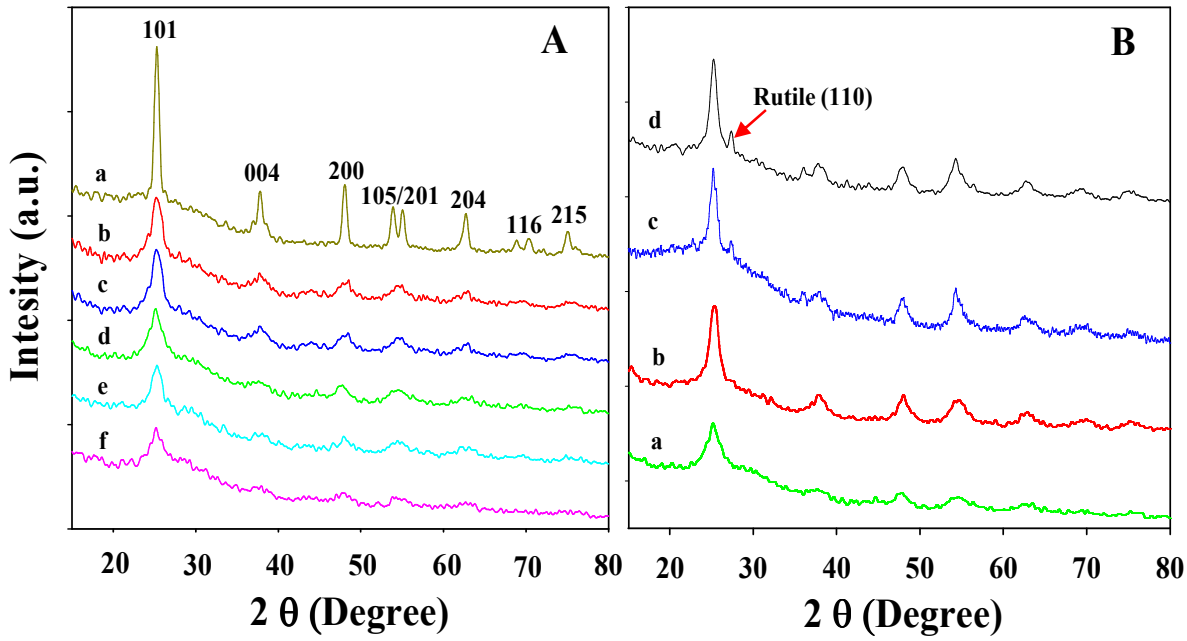

Fig. 2 XRD patterns of (A) the mesoporous C/TiO_2 composites calcined at 450 °C with varied carbon content: (a) M-TiO_2-450, (b) 5C-95TiO_2-450, (c) 10C-90TiO_2-450, (d) 15C-85TiO_2-450, (e) 20C-80TiO_2-450, (f) 30C-70TiO_2-450, and (B) mesoporous 15C-85TiO_2 composites calcined at different temperatures: (a) 15C-85TiO_2-450, (b) 15C-85TiO_2-550, (c) 15C-85TiO_2-650, (d) 15C-85TiO_2-750.

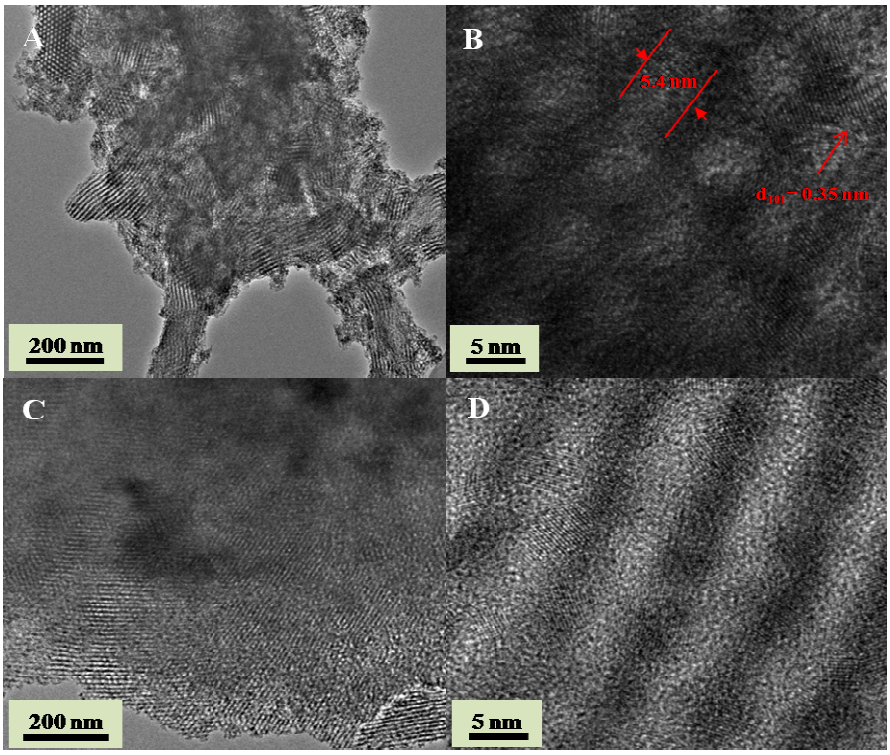

Fig. 3 TEM image (A) and HRTEM image (B) of the ordered mesoporous 15C-85TiO_2-450 composites. TEM image (C) and HRTEM images (D) of the ordered mesoporous 30C-70TiO_2-450 composites.

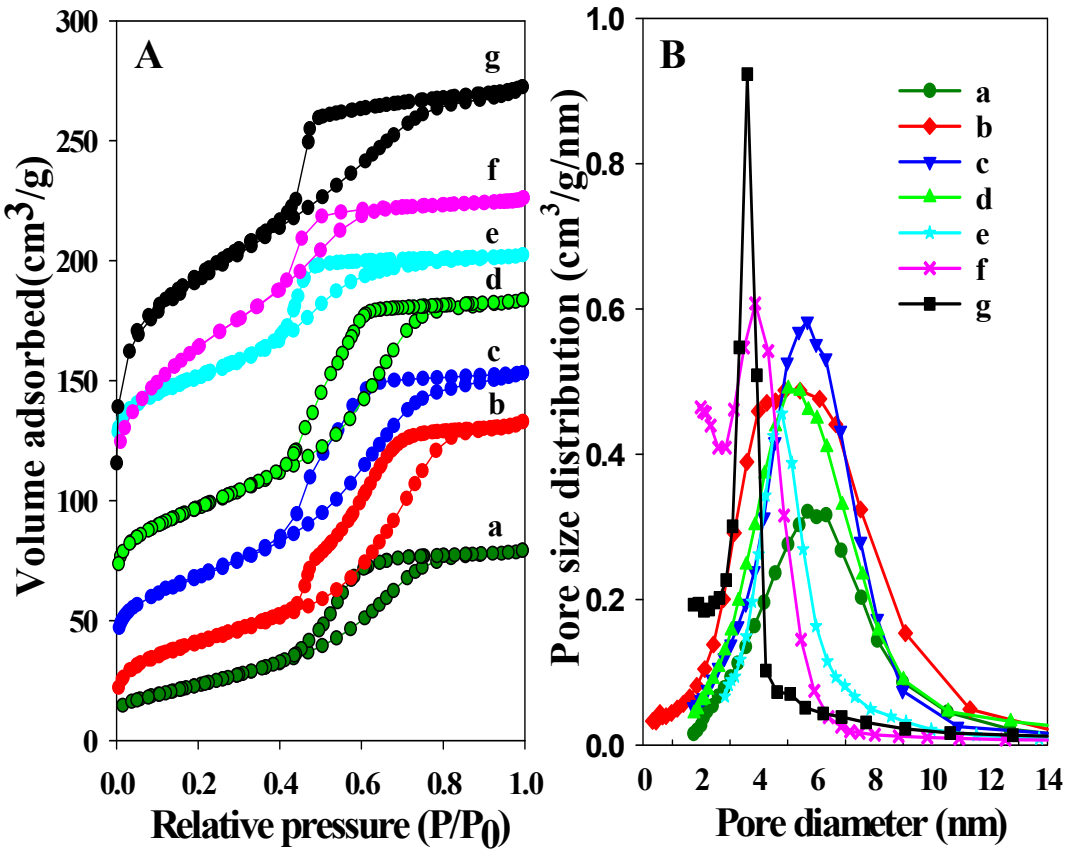

Fig. 4 (A) N_2 sorption isotherms and (B) pore-size distributions of the mesoporous C/TiO_2 composites calcined at 450 °C with varied carbon content: (a) M-TiO_2-450, (b)5C-95TiO_2-450, (c) 10C-90TiO_2-450, (d) 15C-85TiO_2-450, (e) 20C-80TiO_2-450, (f) 30C-70TiO_2-450, (g) C-450**.** In A, the N_2 sorption isotherms of 10C-90TiO_2-450, 15C-85TiO_2-450, 20C-80TiO_2-450, and 30C-70TiO_2-450 are shifted vertically by 30, 50, 60, and 70 cm^3/g, respectively.

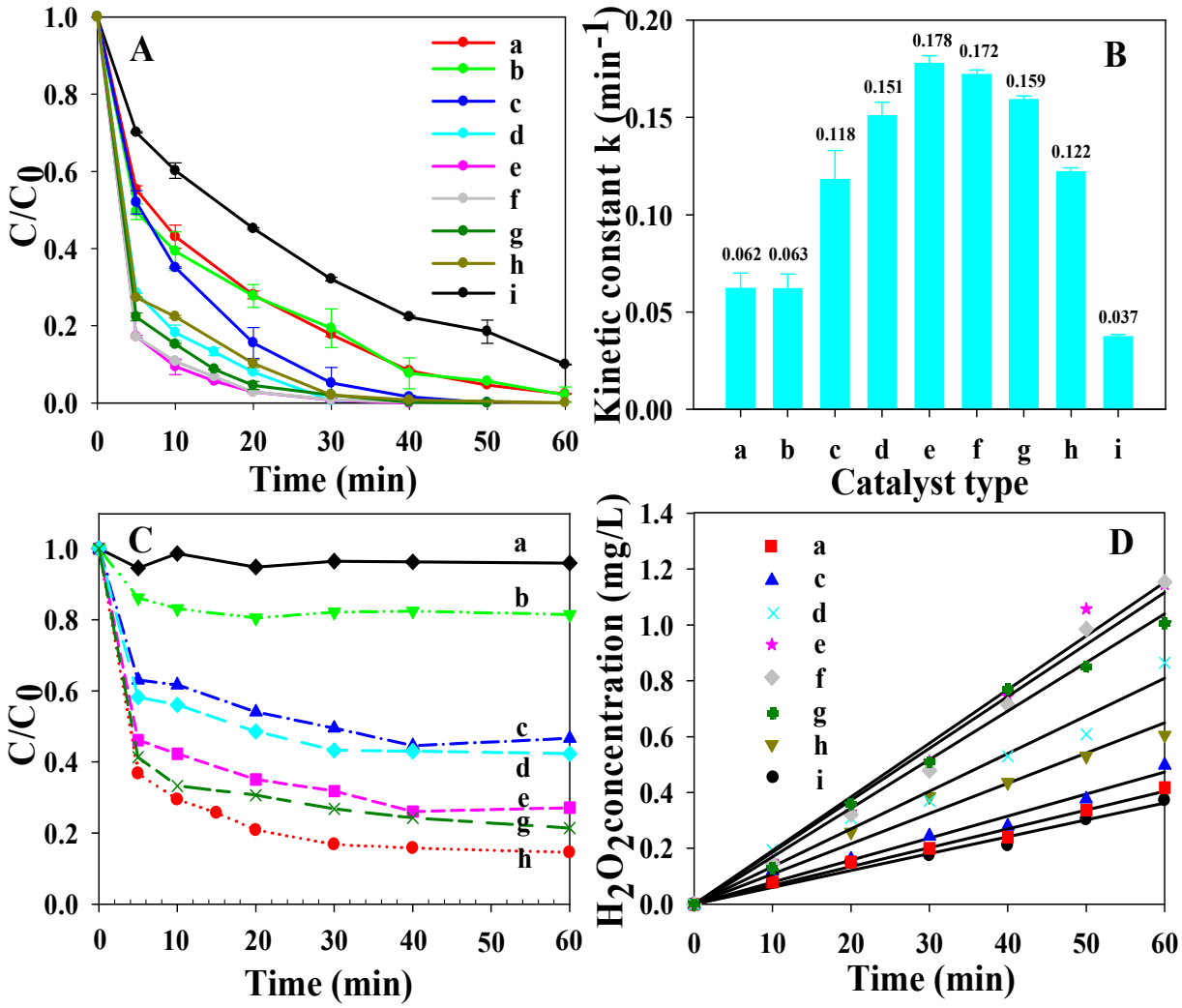

Fig. 5 The sonocatalytic performance of the mesoporous C/TiO_2 composites with varied carbon contents: (A) the degradation profiles of RhB, (B) the sonocatalytic degradation kinetic constants, (C) the adsorption kinetic, and (D) H_2O_2 generation rate. (a) P25, (b) M-TiO_2-450, (c) 5C-95TiO_2-450, (d) 10C-90TiO_2-450, (e) 15C-85TiO_2-450, (f) 20C-80TiO_2-450, (g) 30C-70TiO_2-450, (h) C-450, (i) US alone.

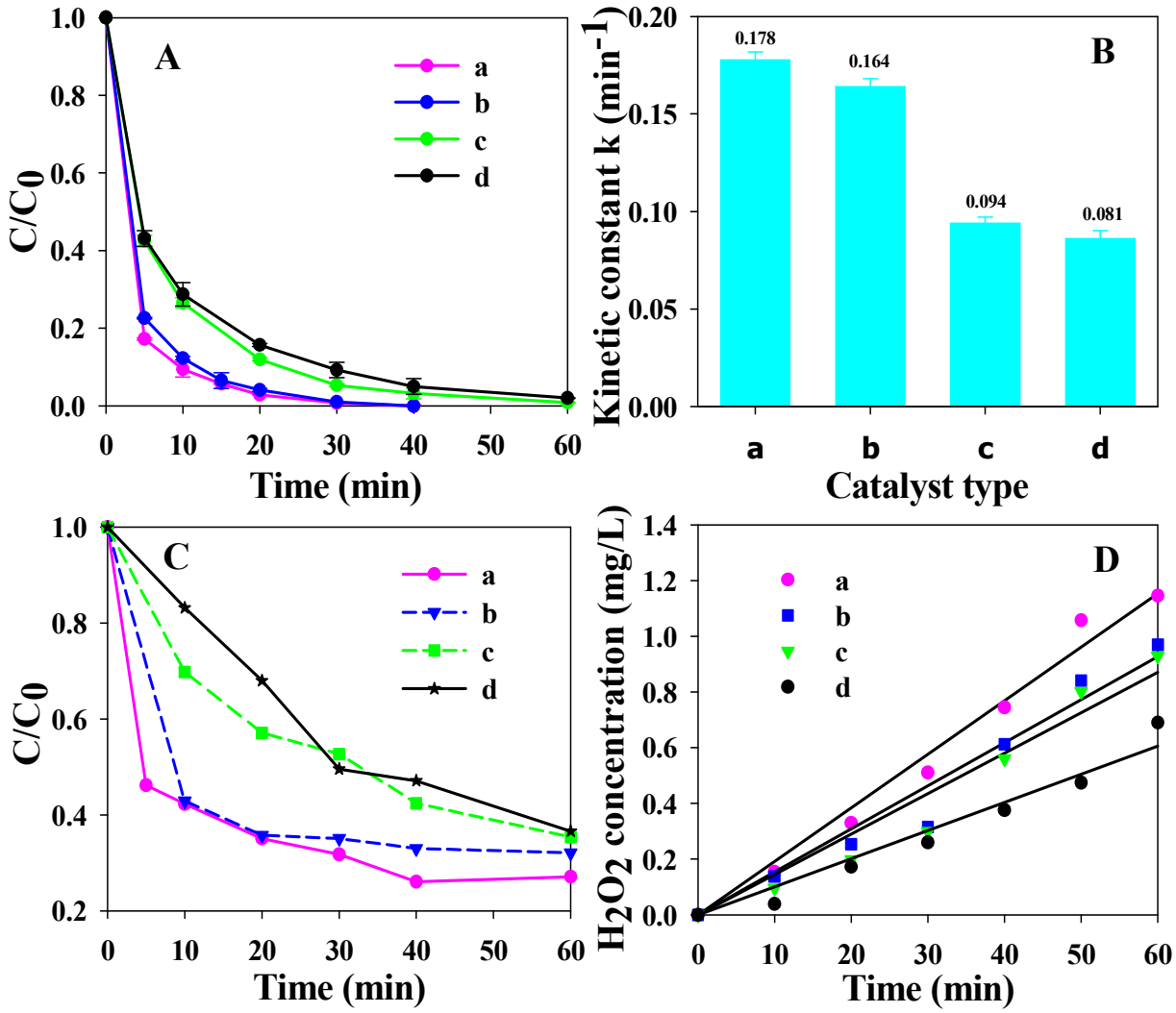

Fig. 6 The sonocatalytic performance of the mesoporous 15C-85TiO_2 composites calcined at different temperatures: (A) the degradation profiles of RhB, (B) the sonocatalytic degradation kinetic constants, (C) the adsorption rate and equilibrium, and (D) H_2O_2 generation rate of (a) 15C-85TiO_2-450, (b) 15C-85TiO_2-550, (c) 15C-85TiO_2-650, (d) 15C-85TiO_2-750.

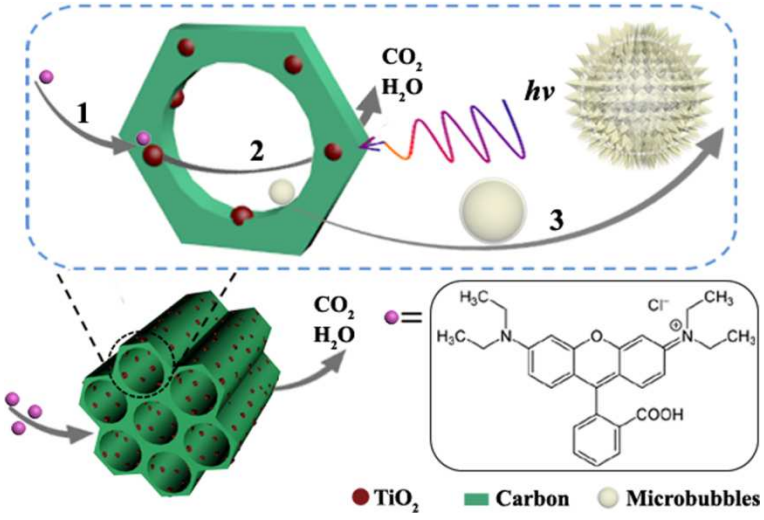

Fig. 7 Illustration of the sonocatalytic degradation process of RhB by using the mesoporous C/TiO_2 catalyst: (1) enhanced mass transfer and adsorption process, (2) Surface redox reaction of the organic pollutants on TiO_2, and (3) pore mediated formation of cavitation bubbles.